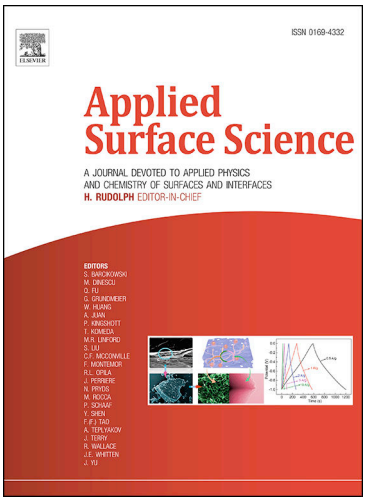
Journal Pre-proofs



Self-build of C_{60}-C_{70} Molecular Heterojunctions on Highly Oriented Pyrolytic Graphite

Lu'an Guo, Yitao Wang, Dogan Kaya, Zhiming Wang, Min Zhang, Quanmin Guo

PII: S0169-4332(20)32899-3
DOI: https://doi.org/10.1016/j.apsusc.2020.148142
Reference: APSUSC 148142

To appear in: *Applied Surface Science*

Received Date: 29 June 2020
Revised Date: 22 September 2020
Accepted Date: 9 October 2020

Please cite this article as: L. Guo, Y. Wang, D. Kaya, Z. Wang, M. Zhang, Q. Guo, Self-build of C_{60}-C_{70} Molecular Heterojunctions on Highly Oriented Pyrolytic Graphite, *Applied Surface Science* (2020), doi: https://doi.org/10.1016/j.apsusc.2020.148142

This is a PDF file of an article that has undergone enhancements after acceptance, such as the addition of a cover page and metadata, and formatting for readability, but it is not yet the definitive version of record. This version will undergo additional copyediting, typesetting and review before it is published in its final form, but we are providing this version to give early visibility of the article. Please note that, during the production process, errors may be discovered which could affect the content, and all legal disclaimers that apply to the journal pertain.

© 2020 Elsevier B.V. All rights reserved.

Journal Pre-proofs

Self-build of C_{60}-C_{70} Molecular Heterojunctions on Highly Oriented Pyrolytic Graphite

Lu'an Guo[a,b,d], Yitao Wang[b], Dogan Kaya[c], Zhiming Wang [d*], Min Zhang [a*], Quanmin Guo[b*]

[a] *Guangdong Engineering and Technology Research Centre for Advanced Nanomaterials, School of Environment and Civil Engineering, Dongguan University of Technology, Dongguan, 523808, China*

[b] *Nanoscale Physics Laboratory, School of Physics and Astronomy, University of Birmingham, Edgbaston, Birmingham, B15 2TT, United Kingdom*

[c] *Department of Electronics and Automation, Vocational School of Adana, Cukurova University, 01160, Cukurova, Adana, Turkey*

[d] *Institute of Fundamental and Frontier Sciences, University of Electronic Science and Technology of China, Chengdu, 610054, China*

Abstract

Building a novel heterojunction with hybrid structures can create new physical properties and enable unique functionality. We investigated the build of C_{60}-C_{70} heterojunction between C_{60} and C_{70} molecular layers by Scanning Tunnelling Microscopy (STM). The C_{60}-C_{70} organic molecular heterojunction was successfully built by layer-by-layer growth method on the HOPG surface using ultra-high vacuum STM. Both molecules can rotate freely within their corresponding molecular layers at room temperature. When C_{70} molecules are deposited onto a preformed first layer of C_{60}, the C_{70} molecules assemble into a close-packed second layer with a lattice-matched to the underlying C_{60} layer. The C_{70} molecules in the second layer adopt a standing up configuration with its long molecular axis perpendicular to the substrate which is accompanied by the elimination of the energy component associated with the rotation around the short molecular axis. C_{70} and C_{60} molecules at layers margins become mobile due to annealing processes and can jump up and form a new packing layer on its origin layer, C_{70}

* Corresponding authors:

Tel: +44 (0) 121 414 4657, Email: q.guo@bham.ac.uk (Quanmin Guo),

Email: mindear@dgut.edu.cn (Min Zhang),

Email: zhmwang@uestc.edu.cn (Zhiming Wang).

molecules remain as isolated molecules standing with their long axis perpendicular to the layers. The C_{60}-C_{70} molecular heterojunctions allow building a lateral/vertical van der Waals heterojunctions.

Key Words: Heterojunctions; Fullerene; Scanning Tunnelling Microscopy; HOPG ; Self-build

1. Introduction

Carbon-based materials are the most studied and exploited due to the versatile ways of bonding between the carbon atoms [1–3]. Highly oriented pyrolytic graphite (HOPG), one of the allotropies of carbon, is a useful solid-state material consisting of large numbers of regularly stacked graphene layers, often used as a subtract in the study of surface science due to its stable, renewable, and an atomically flat surface. Although HOPG, carbon nanotubes, and fullerene molecules are relatively new materials, they have also been extensively studied. The preparation of carbon clusters using laser evaporation, C_n, which is *n* ranges from 2 to 200, has also been extensively studied [2,4]. Among these carbon clusters, C_{60} and C_{70} were investigated for the first time due to their abundance and higher stability [5]. The long axis of C_{70} is about 1.07 times the diameter of C_{60} [6,7], both these two molecules can form single crystals with the fcc structure at room temperature (RT). Thus, it is expected that the two molecules can be mixed to form a binary solid similar to the formation of binary colloidal lattices [8,9]. Binary mixtures of C_{60} and C_{70} in solid solutions have been studied and found that mixing of the molecules can suppress the orientational transition temperatures of the whole system [10,11]. When deposited, both C_{70} and C_{60} onto HOPG they form close-packed molecular layers [12–15]. The growth follows approximately the layer-by-layer growth mode and so this is called two-dimensional layered materials (2DLMs) [16]. The interaction of layers is van der Waals interactions rather than chemical bonding or a strong hybridization with delocalized states, such a C_{60} on Au(111) or PTCDA on conductive n-doped ZnO, which allows us to produce a

vertical/lateral heterojunctions [17–22]. A large number of conjugated π bonds exist in these organic molecules, makes it possible to grow an inorganic material on its surface and form an organic-inorganic van der Waals heterojunctions due to van der Waals interactions [23]. Moreover, the strong hybridization with localized states in a proper substrate or organic molecules, makes these fullerene molecules are promising material exploring and fabricate organic electronics device or single-molecule devices [19,20,23–26]. Besides the similarities between C_{60} and C_{70}, there are clear differences in their geometric structures. While C_{60} has a spherical shape with an icosahedral symmetry [27], C_{70} adopts an ellipsoidal shape due to the extra ten carbon atoms which creates a more complex carbon-carbon bonding. Stacking a C_{60} layer on a C_{70} layer or vice versa introduces strain at the interface. It has been found that the C_{70} molecules can take a particular orientation in order to reduce the interfacial strain, however, the impact of strain and regulatory on the packaging structure still undiscovered [27,28]. Van der Waals Heterostructures, such as the system of C_{60}-C_{70}/Graphene, C_{60}-C_{70}/hBN, and C_{60}-C_{70}/Transition metal dichalcogenide are promising materials for the fabrication of C_{60}-C_{70} molecular heterojunctions [29–31].

The scanning tunnelling microscopy (STM) is a versatile tool to study molecular heterojunctions due to its ability to image surfaces in real space with atomic resolution. The molecular layers of fullerenes were prepared on various substrates, such as Ag, Cu, Au, Al [32,33]; MoS_2 [34,35], graphene [36] and their heterostructures [15,37] and the molecular orientation and structures were revealed by STM at various temperature. The C_{60}/C_{70} heterostructures on graphene surfaces have been rarely studied; there are still open questions such as the formation of C_{60} and C_{70} layer as a function of coverage and elevated temperature. In this paper, we focus on these open questions and report the findings from a recent study of the intermixing of C_{60} and C_{70} on a HOPG surface under ultra-high-vacuum (UHV) conditions in STM. The growth process of C_{60}-C_{70} molecular heterojunctions will be discussed with

different deposition sequences/ratio. Furthermore, the effect of elevated temperature on the C_{60}-C_{70} heterojunction results in self-organize layers and creates a new type of molecular Van der Waals heterostructure.

2. Experimental

The experiments were performed using a room temperature Beetle-type 400 RHK and Omicron variable-temperature STM systems. HOPG (purchased from Goodfellow, 99.99% purity) was used as a substrate and it was annealed before fullerene depositions in UHV at 475 K for 30 min to remove surface contaminations. C_{60} and C_{70} molecules (purchased from MER, 99.5% purity) were deposited onto the HOPG substrate using home-built effusion cells with a rate of 0.12 and 0.10 ML/min, respectively while keeping the background pressure below 10^{-9} mbar. Electrochemically etched tungsten tips were used after high-temperature annealing in the UHV chamber. Images were collected using the constant current mode with a tunnelling current of 0.1 nA and bias voltage in the range between +2.00 V and +2.58 V. For the investigation of molecular mixing, we prepared two samples with sequentially deposited molecules. i) The first sample was deposited with 1.2 ML of C_{60} followed by the deposition of an extra 0.2 ML of C_{70}. ii) The second sample was deposited with 1.2 ML of C_{70} followed by the deposition of an extra of 0.2 ML of C_{60}. In each case, the substrate temperature was gradually elevated up to 475 K.

3. Results and Discussions

3.1 Deposition of 1.2 ML C_{60} (and C_{70}) on HOPG

Fig. 1(a) shows an STM image of the first sample with 1.2 ML C_{60} deposition on HOPG at room temperature. The image shows the formation of the first layer with the C_{60} array and the second layer with dendritic-island structures. We observed two incomplete layers of C_{60} island formations. The first layer formed directly above HOPG that covers ~78.6% of the substrate. The second layer of C_{60} island forms on the top of the first layer. Although the total coverage is greater than one monolayer, there is still a small fraction of bare graphite areas that

is because the second layer starts to form before the first layer is completed. The adsorption energy of C_{60} on top of a C_{60} layer is calculated to be 968 meV which is slightly higher than the 813 meV adsorption energy of C_{60} on HOPG surface [38]. The diffusion barrier for the C_{60} molecule on HOPG surface is only 13 meV, which is much lower than the C_{60} energy barrier on a C_{60} layer of 168 meV [38]. Therefore, the C_{60} molecules diffuse long-range on HOPG surface at RT so the first layer of C_{60} is expected to adopt a thermodynamic equilibrium shape. The dendritic-island structure of the second layer of C_{60} is a result of diffusion-limited growth due to the much higher diffusion barrier. Applying simple triangulation on high-resolution images, we can identify that the second layer molecules occupy the three-fold hollow site of the first layer. Figs. 1(c and d) is the magnified view of the areas in Figs. 1(a and b) with a ball model, respectively. The overlapped yellow and blue balls in the image illustrate the first and second layers of molecules on HOPG surface, respectively. It shows a schematic ball model that illustrates the positional relationship between the first two C_{60} layers. This layer is probably growth an fcc orientation by further deposition of C_{60} molecules. The azimuthal orientation of the C_{60} molecular rows relative to the HOPG is not analysed here. This is because it hard to obtain high-resolution images of both the C_{60} layer and HOPG substrate by STM simultaneously [39].

The STM images in Fig. 1(b) show HOPG substrate, the first and, the second layer of C_{70} after deposition of 1.2 ML of C_{70} on HOPG surface at RT. Similar to the growth of the C_{60} mechanism, the second molecular layer is formed before the first layer is completed. The C_{70} molecules at the edges of the second layer are diffuse at RT. Dendritic-island structures are also observed for the second layer of C_{70} island. Due to the weak van der Waals interaction between molecules and the effect of the electric field below the tip apex [40,41], the C_{70} molecules are found to be freely diffuse on the surface and around the island at RT. Therefore, the shape of the second layer islands gradually changes in time while the surface is being

imaged under the STM. The inset plot in Fig. 1(b) shows a height profile which is measured along the blue line A-B. Based on this height profile, the first and second layers are 1.00 nm and 1.80 nm above HOPG surface, respectively. This difference is due to the second layer spheres sitting in the three-fold hollow site of the first layer. Similarly, the first and second layers of C_{60} are 0.80 nm and 1.50 nm above HOPG surface, respectively. Due to the elongated shape of the C_{70} molecule, it rotates on both surface and molecular island. For a free rotating ellipsoidal molecule, it has an effective diameter which corresponds to the measured height of the molecules as 1.00 nm. A C_{70} molecule stands on HOPG surface perpendicular to the substrate with its long axis appears higher than 1.00 nm. The C_{70} molecules within the second layer occupy the three-fold hollow site of the first layer.

Journal Pre-proofs

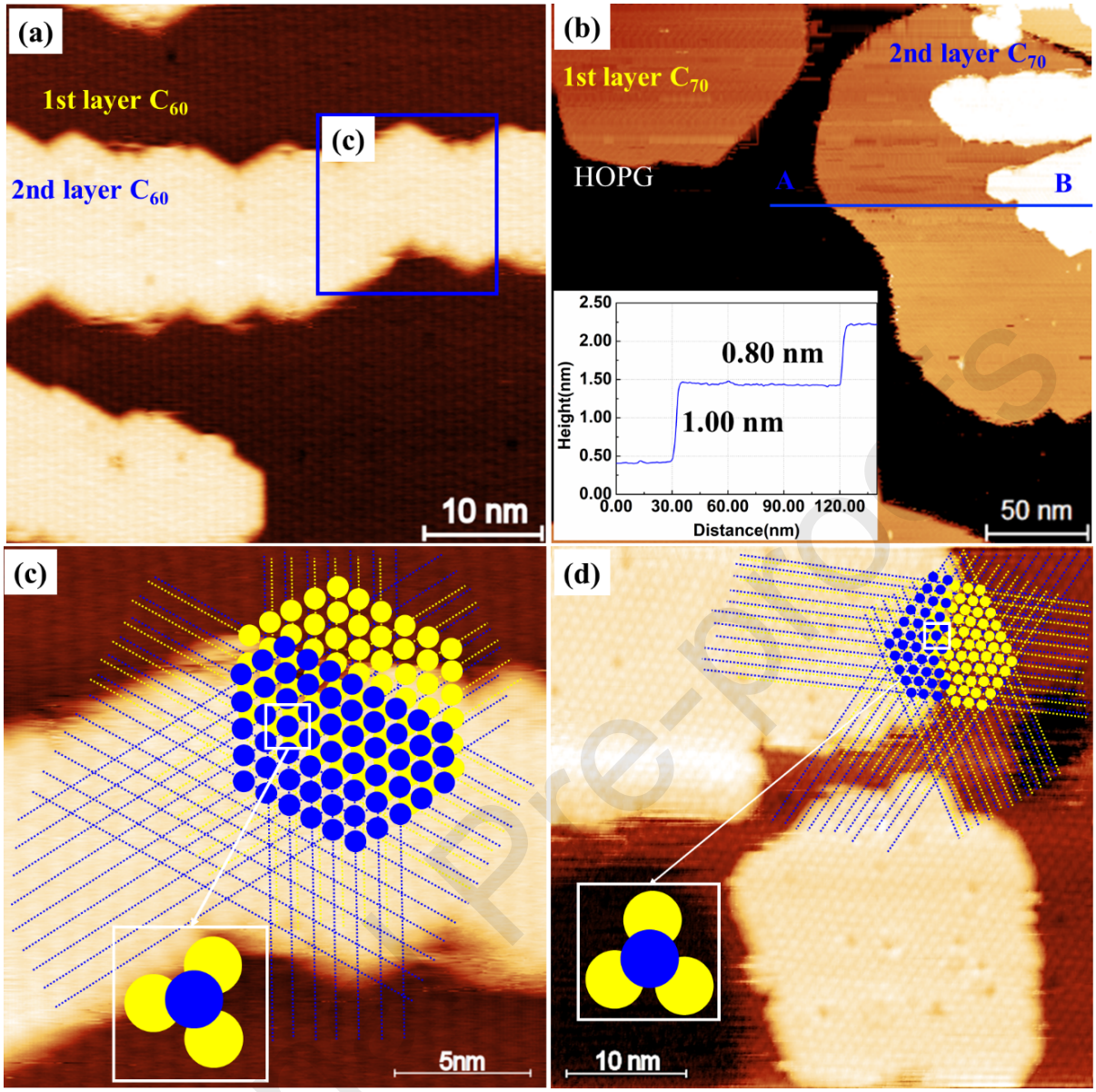


Fig. 1. 1.2 ML deposition of C_{60} and C_{70} molecules on HOPG surface at room temperature. (a) An area of HOPG showing a large fraction of the surface covered by a single layer of C_{60} with an existence of the second layer of C_{60} island. (b) A large area STM image shows the co-existence of bare HOPG surface, the first layer, and the second layer of C_{70} islands. The inset plot shows the height profile of the first and the second layer of C_{70} island along the blue A-B line. (c) A selected area (blue square) in (a) showing the details of the step edge structure of the C_{60} dendritic island. (d) Ball model superposed on the top of an STM image for C_{70} island formations. (c and d) Yellow and blue balls are superposed on the top of the STM image to illustrate the positioning of the first and the second layers, respectively. The dashed lines help to determine the occupation site of the second layer molecules.

3.2 Adding 0.2 ML C_{70} (and C_{60}) to an existing 1.2 ML C_{60} (and C_{70}).

Figs. 2(a and b) show STM images that are collected from the sample after adding 0.2 ML of C_{70} (and C_{60}) molecules on 1.2 ML of C_{60} (and C_{70}) molecular island on HOPG, denoted by C_{70}-C_{60}/HOPG and C_{60}-C_{70}/HOPG heterojunctions, respectively. As can be seen in Fig. 2(a), the C_{70} molecules are attached to the edges of the pre-formed C_{60} islands. Each C_{60} island becomes enclosed by a rim with a quite uniform width of C_{70} molecules on the second layer. The C_{70} rim follows exactly the contour of the existing C_{60} island. Hence, the addition of C_{70} does not affect the shape of the C_{60} island and there exists a clear sharp boundary between the C_{60} island and the C_{70} rim. For the first layer, the additional C_{70} molecules also form a rim, but the width of the rim is rather non-uniform. In some areas, the rim is just one or two molecules wide, whereas, in other areas, it is more than 10 molecules wide. The non-uniform width of the rim in the first layer is consistent with the high mobility of C_{70} molecules on HOPG surface. Therefore, molecules were already captured by the island and can diffuse along the edge. On the second layer, it is more likely capture and sticks situation. The mixing of the two molecules has taken place in the first layer so the boundary between the C_{60} island and the C_{70} rim is fuzzy on the first layer. It is expected that the edge of the first layer is rather fluidic with molecules constantly leaving and joining under RT.

The enlarged area (blue square) in Fig. 2(a) is presented in Fig. 2(c). The edge of the second layer of C_{60} creates a smooth region of C_{70} arrays and this C_{70}-C_{60} formation is confirmed by the height profile along the blue line C-D in the inset plot. The C_{70} rim in the second layer is 0.80 nm above the 1st layer C_{60}. This is 0.11 nm higher than C_{60} molecules within the same layer. This line profile also confirms that the C_{70} molecules form a natural extension from the existing C_{60} layer with no lateral defect among island except that the height of the C_{70} molecule is higher. It also shows that the nearest neighbour distance that is measured as 0.99 nm on three directions for both C_{60} and C_{70} molecules. Therefore, C_{60} and C_{70} molecules in the second layer occupy the same type of hollow site. This further suggests that C_{70}

molecules sitting above a C_{60} layer that provides their molecular axis perpendicular to the surface in order to fit the lattice parameters of the underlying C_{60} layer. We find that for the first C_{70} layer, the nearest neighbour distance is 1.14 nm whereas, for the first layer C_{60}, the nearest neighbour distance is 1.05 nm. These nearest neighbour distances are consistent with the lattice parameters for C_{70} and C_{60} crystals at RT.

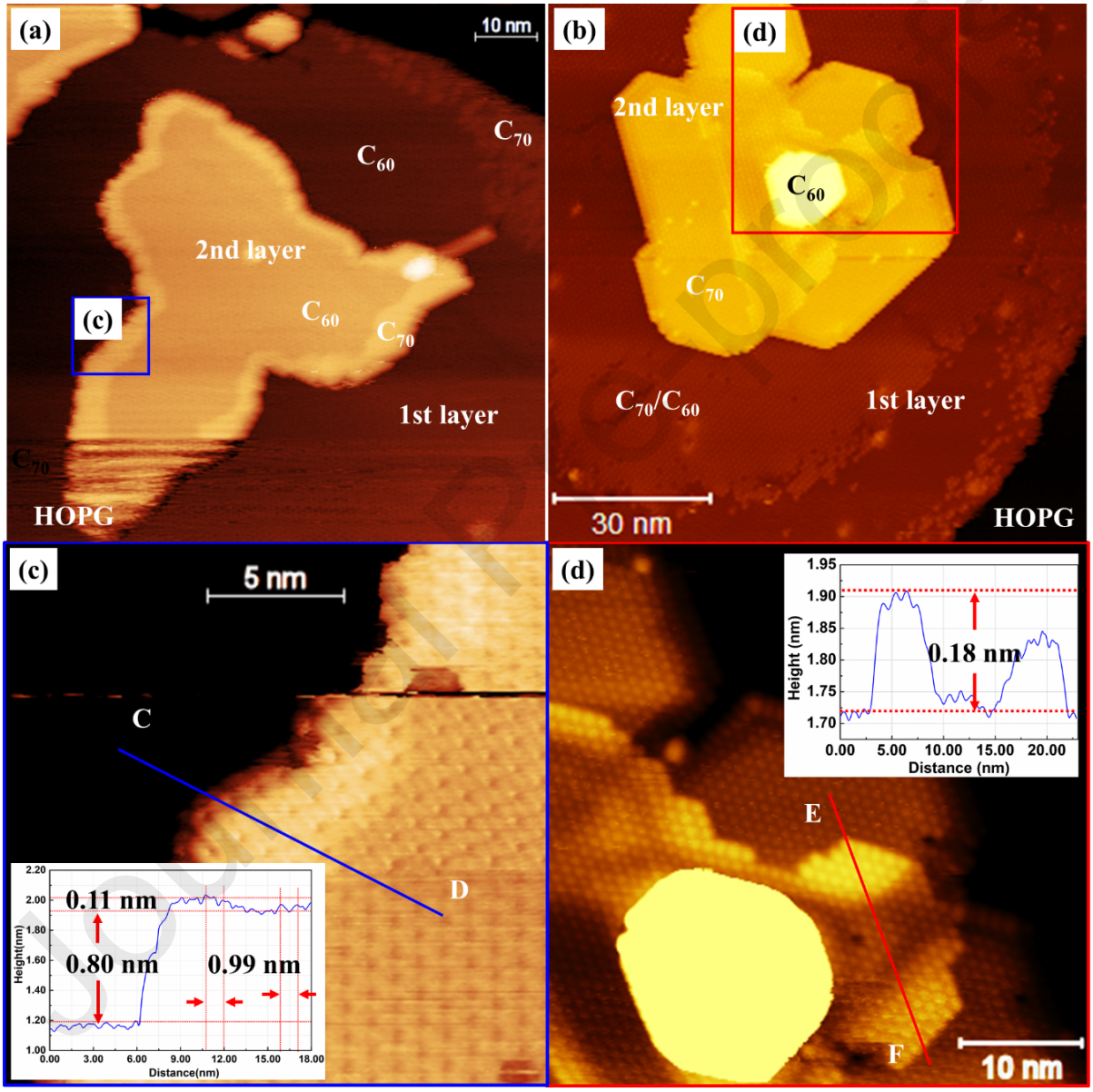


Fig. 2 (a and b) 0.2 ML of C_{70} (C_{60}) added onto an existing 1.2 ML of C_{60} (C_{70}) on HOPG at RT, respectively. For C_{70}-C_{60}/HOPG mixture in (a), C_{70} molecules attach to the edges of the C_{60} island, and form rims in both the first and the second layers. For C_{60}-C_{70}/HOPG mixture in (b), the first, second and third layers form C_{70}-C_{60} mixture, C_{70}, and C_{60} islands. (c and d) The blue and red squares in (a and b) show enlarged areas of C_{70}-C_{60}/HOPG and C_{60}-C_{70}/HOPG

formations, respectively. The inset plots are the height profile along line C-D and E-F that show the height differences of 0.11 and 0.18 nm, respectively.

For comprehensive and systematic study, we changed the deposition sequence. Fig. 2 (b) shows the deposition of the first layer of 1.2 ML of C_{70} on HOPG and then adding 0.2 ML of C_{60} at RT. The C_{60} molecules are found to form a close-packed C_{60} layer enclosing the preformed C_{70} islands on both the first and the second layers. A small patch of C_{60} is formed on top of the second layer C_{70}. Intermixing has clearly taken place at the C_{70}/C_{60} boundary in the first layer. Formation of such a boundary is expected if the edges of the initial C_{70} island consist of mobile molecules. Hence, a significant number of C_{70} molecules can detach, diffuse, and from C_{70} island at the edges and near the island at RT. When the C_{60} molecules are added, they mix with the mobile C_{70} molecules at the edge. Therefore, the final structure consists of a pure C_{70} and C_{60} regions, and a narrow region were mixed with C_{60} and C_{70} molecules sandwiched in between. From the image in Fig. 2(b), one can be estimated the distance that a C_{70} molecule can diffuse when it manages to escape from the edge of the C_{70} island. Here the average distance is about 5-6 nm. Thus, a C_{70} island on HOPG at RT is in equilibrium with its "fluidic (vapor-like)" which extends 5-6 nm [28]. Once the boundary is formed, no further cross-boundary diffusion can take place at RT. For C_{60} molecules inside the C_{70} array, there is a high tendency that C_{60} molecules group together forming a short row of C_{60} island formation. There could be several reasons why C_{60} form rows inside the C_{70} layer. First, the preferred directional of C_{60} bonding could be one of the reasons. However, considering that orientational ordering within C_{60} and C_{70} arrays are destroyed by thermal energy at RT, therefore it is unlikely that directional bonding drives the formation of the C_{60} rows. Second, more likely reason is associated with a strain induced formation by the insertion of C_{60} into the C_{70} layer. One single isolated C_{60} molecule inside a C_{70} layer disturbs the bonding of six C_{70} molecules. By forming a row, the number of affected C_{70} molecules per C_{60} molecule could be minimized. In the second layer, an axial molecular formation between C_{60} and C_{70} were shown in the

enlarged image (red square) in Fig. 2(d). Thus, the edges of the C_{70} islands in the second layer are more stable. There might still be the step edge diffusion, but no C_{70} molecules can escape from the edges of the island.

Deposition C_{70} molecules on the C_{60} layer result in a simple epitaxial growth without changing the island formation of the C_{60} layer. On the other hand, the deposition of C_{60} molecules on the C_{70} layer is a more complicated system because C_{60} molecules can penetrate in the C_{70} layer. This increases the molecular density of the first C_{70} layer and forces some C_{70} molecules to stand up with the long molecular axis perpendicular to the substrate. Placing a close-packed C_{60} layer on top of a C_{70} layer also causes re-organize the C_{70} layer [28]. The nearest neighbour distance of C_{70} is found to be 1.07 nm which is large enough for C_{60} molecules to rotate at RT. As a result, when the second C_{60} layer is formed on top of the first C_{70} layer, the compressive stress causes the free-rotating and the C_{70} molecules take an upright position with the long molecular axis perpendicular to the substrate creating a lattice-matched C_{60}/C_{70} interface. The change of orientation of C_{70} molecules creates extra space within the first layer which is then filled by C_{60} molecules [28]. As can be seen in Fig. 2(d), the height profile of C_{70} molecules in the second layer from E to F is rather non-uniform due to the change to the first layer. In the absence of C_{60}, the second layer of C_{70} has a uniform height as already shown in Fig. 1(d).

3.3 Thermally activated structural evolution

Following, we investigated how the structures of the C_{70}-C_{60}/HOPG and C_{60}-C_{70}/HOPG heterojunctions were responded to the elevated substrate temperature. Therefore, we annealed the samples for 30 minutes at a fixed temperature (range from 375 K to 475 K) and then cooled down to RT followed by STM imaging. Fig. 3(a) shows the morphology of the C_{70}-C_{60}/HOPG heterojunctions after annealing at 375 K for 30 minutes. The C_{70} rim in the first layer is broken due to the inward movement of the C_{70} molecules. Some C_{70} molecules have also diffused into

the C_{60} layer more than 10 nm. As mentioned before, there is a "vapor-like" phase in equilibrium with the "solid" first layer due to the elevated temperature. Annealing the sample at 375 K creates a mixture of C_{60} and C_{70} island in this vapor-like phase. After annealing, this phase condenses into the solid phase. The second layer formation shows a clear boundary between C_{60} and C_{70} molecular arrays. It can be concluded from Fig. 3(a) that the vapor-like phase at 375 K reaches a distance of ~ 10 nm in the layer. The bulk of the first layer remains in the solid phase during annealing. Hence the second layer in Fig. 3(a) retains its shape. A third layer island is formed in the area inside a red square. The height of the 3rd layer island is given in the enlarge image (red square), the line G-H (blue line) is 0.86 nm which is consistent with the height profile of the C_{70} molecule. Therefore, during annealing, some C_{70} molecules have managed to diffuse up the step edge and aggregated into a third layer island.

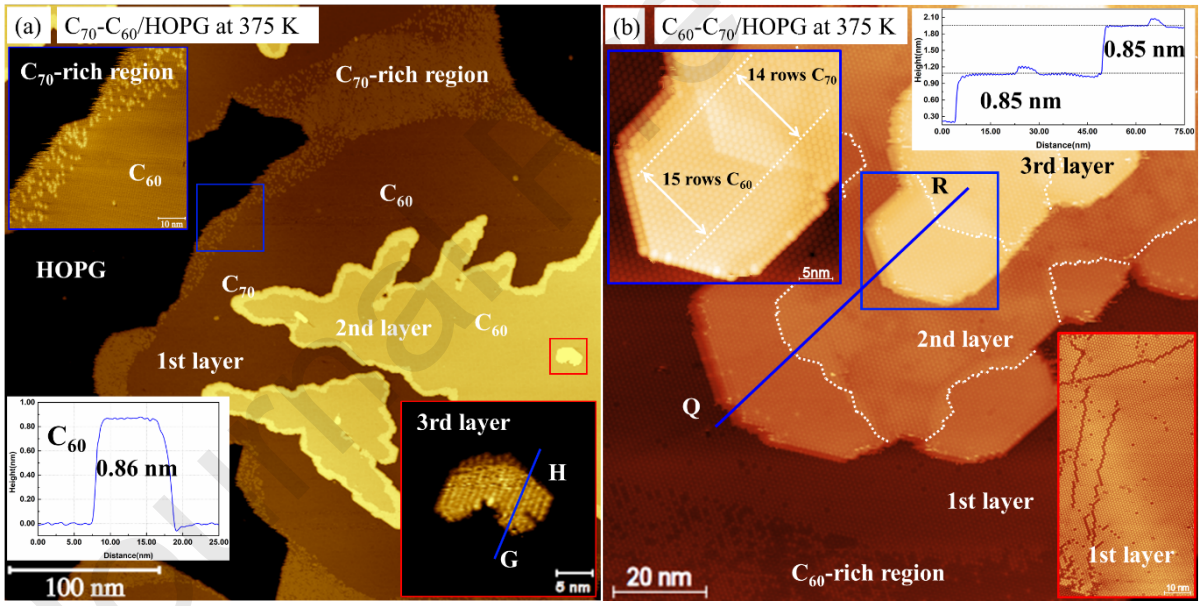


Fig. 3. The morphology of C_{70}-C_{60}/HOPG and C_{60}-C_{70}/HOPG formations after annealing at 375 K for 30 min. (a) The sample of C_{70}-C_{60}/HOPG, the enlarged areas, blue and red squares, show diffused C_{70} molecules in C_{60} island and individual C_{70} island on the top of the second layer, respectively. The height profile of the 3rd layer of C_{70} island is measured as 0.86 nm along the line G-H (blue line). (b) The sample of C_{60}-C_{70}/HOPG, the red square shows the area incorporation of C_{60} molecules into the C_{70} layer. The enlarged area (blue square) shows a large C_{70} island on the third layer. The white dotted lines indicate the trace of the domain-boundaries.

The height profile of the 2nd and 3rd layer of C_{60}-C_{70} island were measured as 0.85 nm along the line Q-R (blue line)

For the C_{60}-C_{70}/HOPG sample were prepared by adding 0.2 ML of C_{60} onto a pre-formed 1.2 ML C_{70}, the surface morphology after annealing at 375 K is shown in Fig. 3(b). There are now more C_{60} molecules incorporated into the 1st C_{70} layer which form a C_{60}-rich region. Some of the incorporated C_{60} molecules form dark zig-zag rows as shown in the inset image at the bottom right of Fig. 3(b). The inset height profile in the Fig. 3(b) shows a clear increase on the white dashed line which is correspond to the C_{70} molecules. The structures of the second and third molecular layers provide rather complex formations. There are boundaries in each layer as shown by white dotted lines. By draw two parallel lines crossing both sides, they are accommodates 14 rows of C_{70} and 15 rows of C_{60}, two parallel lines, showing in the insect of Fig.3(b)[28]. However, there are no clear height differences between molecules on the two sides of a boundary except the pronounced height differences on the boundary, height profile showing in the insect of Fig.3(b).

Fig. 4(a) shows the STM images of C_{70}-C_{60}/HOPG sample acquired after annealing samples at 425 K for 30 min. The first layer now consists of even more C_{60} molecules and has C_{60}-rich and C_{70}-rich regions. Within the C_{60}-rich region, we observe mainly isolated C_{70} molecules close to the rim. These isolated C_{70} molecules take the upright configuration which is confirmed by the height profile. For such a configuration, the C_{70} molecule has the same footprint as C_{60}, therefore, there is no distortion of the C_{60} lattice. Within the C_{70}-rich region, there are individual C_{60} molecules as well as chains of C_{60} as shown earlier in Fig. 3(b). In comparison with images shown in Fig. 3(b) and Fig. 4(b), the morphology of C_{60}-C_{70}/HOPG has not changed much by increasing the annealing temperature from 375 K to 425 K. The height profile in Fig. 4(c) is measured along line I-J (white line) from a C_{60}-rich region in the first molecular layer of Fig. 4(b). The C_{70} molecules, bright spots, are 0.11 nm higher than C_{60}

molecules in the same layer. This suggests that the C_{70} molecules inside the C_{60}-rich region stand upright positions which are the long molecular axis perpendicular to the substrate.

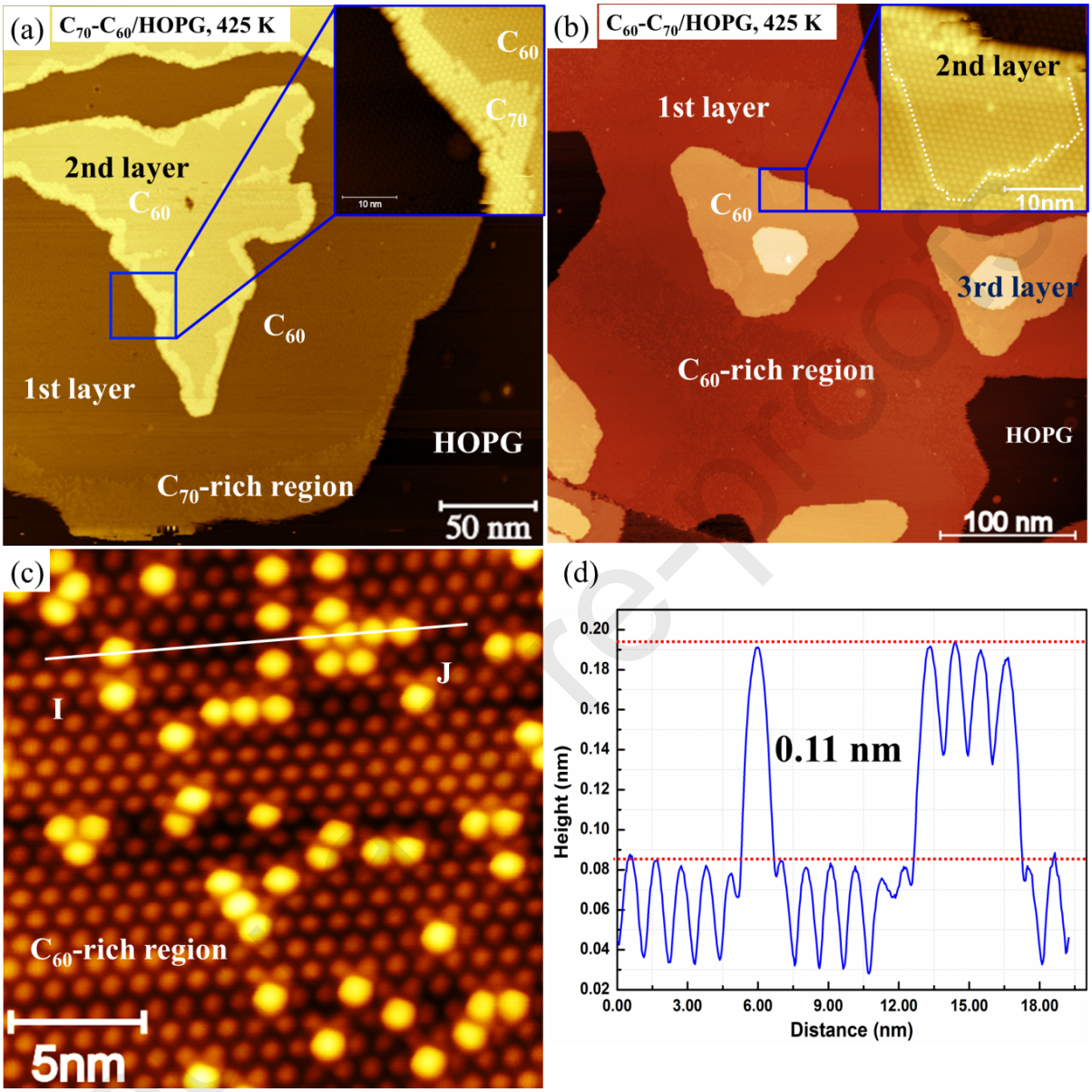


Fig. 4. The morphology of C_{70}-C_{60}/HOPG (a) and C_{60}-C_{70}/HOPG formations after annealing at 425K for 30min. (a) The enlarged inset image of the selected (blue square) shows the formation of C_{70} island as a second layer. (b) The enlarged inset image (red square) in the second layer is formed of the C_{60} layer. (c) A representative C_{60}-rich region of the first layer in the upper area of (b). (d) The height profile along line I-J (white) is plotted in (c) shows 0.11 nm peaks for C_{70} molecules.

Fig. 5 shows C_{70}-C_{60}/HOPG and C_{60}-C_{70}/HOPG formations after annealing at 475 K for 30min. The molecular formation of the first, second, and third layers on HOPG in Fig. 5(a)

were confirmed by the height profile along the surface from K to L which is presented in Fig. 5(c). The blue, red, and green areas in Fig. 5(a) were enlarged at the bottom of Fig. 5(a) for improved resolutions. Fig. 5(b) shows different areas of annealing processes at 475 K. The height profiles, which M to N and O to P lines, of blue and red areas in Fig. 5(b) were enlarged to confirm the molecular formation in Fig. 5(d). Substantial changes of the morphology of the molecular layers were observed after annealing the samples at 475 K. Most notably, the appearances of relatively large molecular islands were observed in the third layer and also dispersed the C_{70} rim in the second layer. Although there are two third-layer islands in the image in Fig. 5(a), a small number of 4th layer islands are also observed. The formation of the 3rd and 4th layer islands require vertical upwards transportation of molecules. Since the binding of molecules to the HOPG substrate is weaker than C_{60}-C_{70}, C_{60}-C_{60}, and C_{70}-C_{70} molecular interactions, the thermally induced molecular diffusion from the first layer to the upper layers is expected to take a place. The stronger inter-island interactions result in multilayers growth. It is interesting to see that the latest formed third layer consists of C_{60} and C_{70} molecules from the inner and outer regions of the mixed island. We did not image the surface during heating of the sample, and thus there is no direct observation as to how the third layer island is formed. During thermal annealing, both C_{60} and C_{70} molecules diffuse to the upper layers that are probably Ostwald ripening mechanism driven by elevated temperature.

At 475 K, the C_{60} and C_{70} molecules probably diffuse between the layers. The 3rd layer islands are likely formed during annealing and the cooling down to RT. If C_{60} molecules switch to the condense phase from a vapor-like phase before C_{70}, we may probably see the phase-separation on the 3rd layer islands with C_{70} decorated island. The shape of the second layer islands forms like-hexagon island formation with more smooth edges that is because the thermally activated of C_{70} molecule diffusion at the edge of the island. The C_{70} rim in the second layer has disappeared through some reorganization leading to less well-defined

boundaries between the C_{60} and C_{70} molecules but there is clearly intermixing of C_{70} and C_{60} molecules around the rim. The dendritic-island structure as seen in Fig. 3(a) for the second layer of the islands has disappeared due to elevated temperature to 475 K. For C_{60}-C_{70}/HOPG, there is significant molecular exchange between the layers. In Fig. 5(b), the second layer islands consist of pure C_{70} with C_{60} molecules almost completely diffuse down to the first layer.

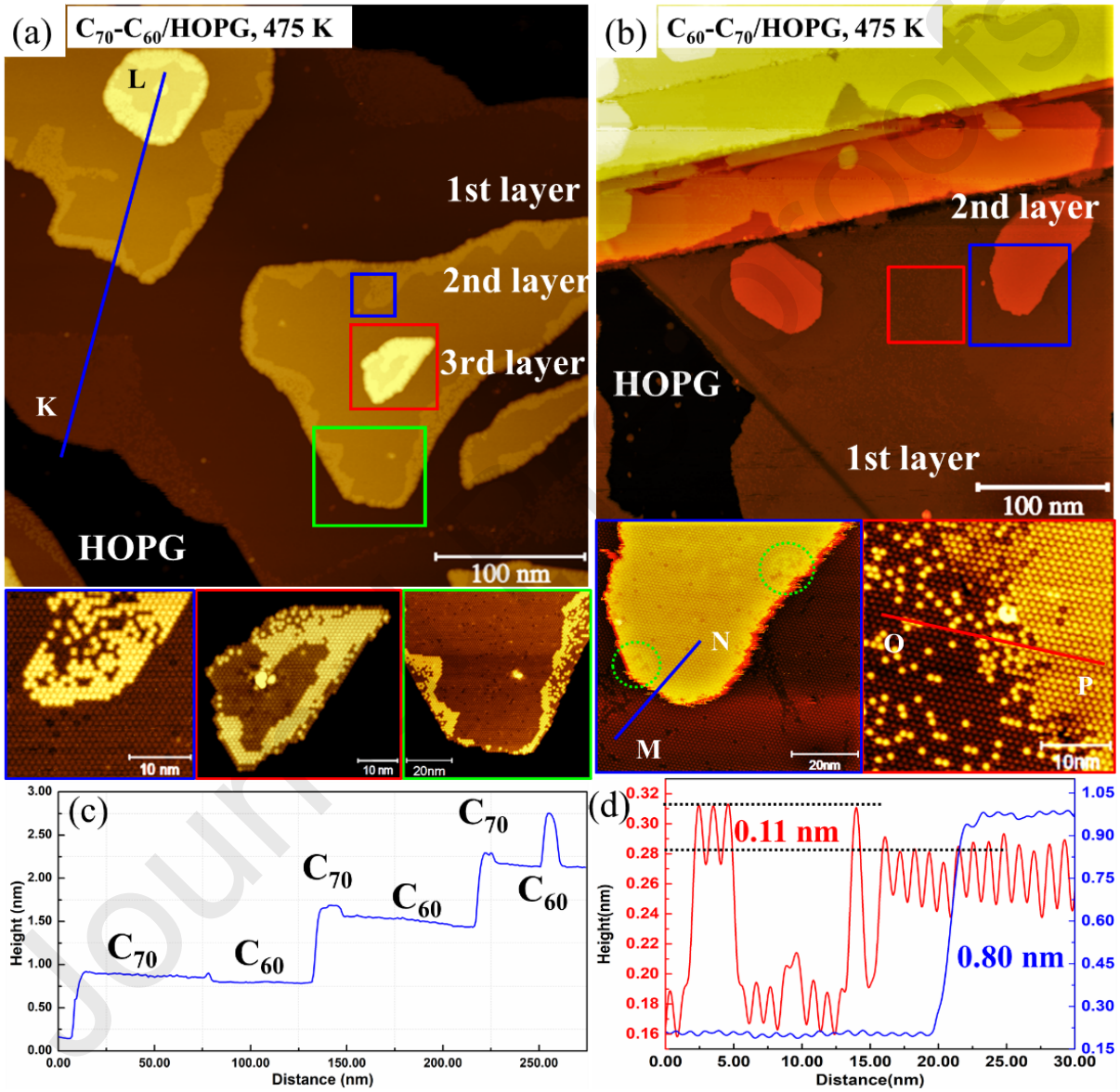


Fig. 5. C_{70}-C_{60}/HOPG and C_{60}-C_{70}/HOPG after annealing at 475 K for 30min. (a) C_{70}-C_{60}/HOPG heterojunctions. The height profile along line K-L (blue) is plotted in (c). The enlarged areas, blue, red, and green squares show the formation of the layers with the mixing of C_{60}-C_{70}. (b) C_{60}-C_{70}/HOPG heterojunctions. The height profile along line M-N (blue) and O-P (red) are plotted in (d).

3.4 Structural models

After performing experiments at different coverages/sequences and annealing temperatures, we propose the structural models for C_{70}-C_{60}/HOPG and C_{60}-C_{70}/HOPG formations. Fig. 6(a) and (c) show the statistical coverages of the 1st, 2nd, and 3rd layers of C_{70}-C_{60} heterojunctions as a function of temperature and Figs. 6(b) and (d) show the ball model the formation of C_{70}-C_{60} heterojunctions. For C_{70}-C_{60}/HOPG formation, we have an incomplete first layer of C_{60} sitting on HOPG, and C_{70} molecules have attached the edges of the C_{60} islands (see Fig. 6(b)). In the second layer, the C_{60} islands were enclosed by C_{70} rims in which the C_{70} molecules take an upright configuration as shown in Fig. 5(c) to keep a lattice-matched interface. Fig. 6(a) demonstrates the thermal annealing outcomes; the first C_{60} layer remains mostly stable. There is upward molecular transport that leads to the formation of third layer islands while both C_{60} and C_{70} molecules appear in the third layer. For C_{60}-C_{70}/HOPG in Fig. 6(d), the C_{70} molecules and the first C_{70} layer (as the 1st and 2nd layers) rotate freely on HOPG, respectively. The height of C_{70} molecules, which were determined by STM images, reflect an effective height of rotating molecules as seen in Fig. 5(d). After adding C_{60} molecules, a lattice mismatch between the first C_{70} layer and the second C_{60} layer appears. The form of the C_{70} molecules changes from a random rotating state to an upright configuration. This makes it difficult to distinguish the formation of the molecular layers as shown by the unevenness of the layers. Heating the sample causes the C_{60} molecules to diffuse into the first layer and some C_{70} molecules in the first layer move up to the second layer.

Journal Pre-proofs

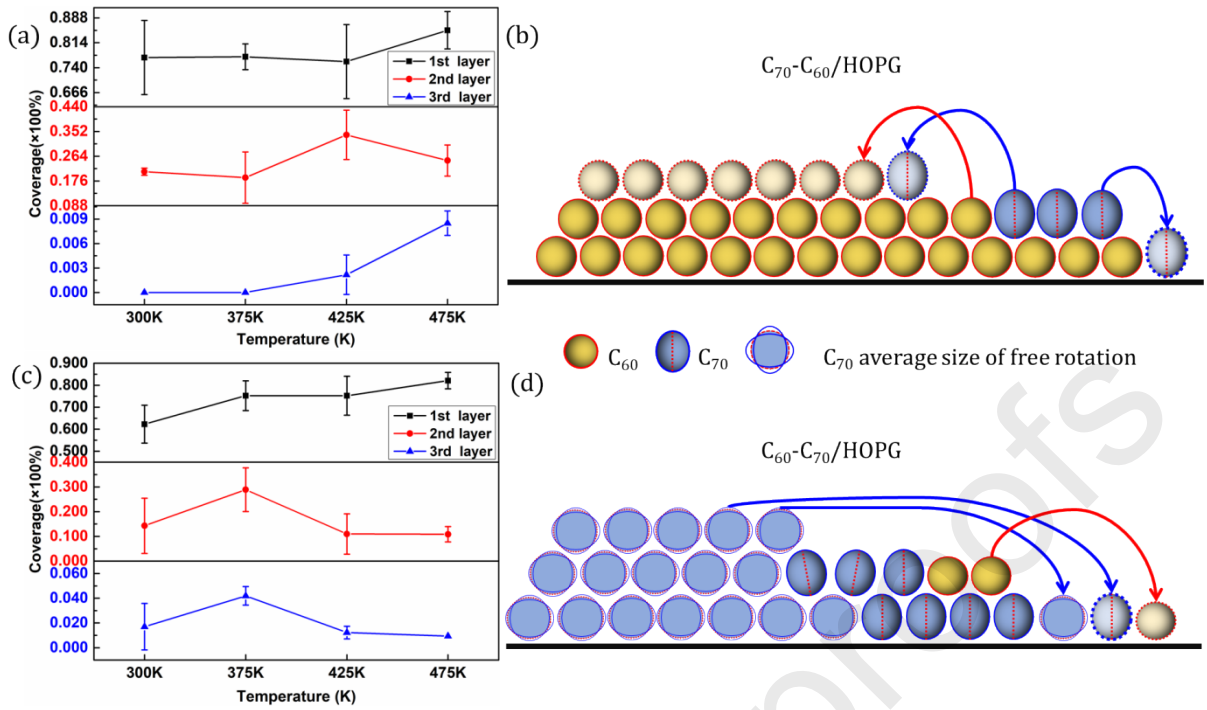


Fig. 6. C_{70}/C_{60} coverage changing with annealing temperature and structural models. (a-b) for C_{70}-C_{60}/HOPG, (c-d) for C_{60}-C_{70}/HOPG. C_{70} molecules on top of a C_{60} layer form a lattice-matched interface by taking an upright configuration. C_{60} molecules on top of a C_{70} layer is able to change C_{70} from a random rotating state to an upright position state. The molecular coverage for the 1st, 2nd, and 3rd layers as a function of temperature are plotted in (a) for C_{70}-C_{60}/HOPG and (c) for C_{60}-C_{70}/HOPG.

4. Conclusions

In summary, the van der Waals heterojunction between C_{60} and C_{70} molecular layers was studied at different coverages/sequences and temperatures. Adding C_{70} to an existing C_{60} layer or vice versa is a possible preparation method for the van der Waals heterojunction applications. When C_{70} molecules are added to a C_{60} layer, C_{70} molecules occupy the three-fold hollow site and form a lattice-matched interface. The lattice match forces the C_{70} molecules to take a fixed upright configuration with a long molecular axis perpendicular to the interface. We observed that the C_{70} molecules also form a close-packed molecular layer and the molecules rotate freely on HOPG at RT. When C_{60} molecules are added to a C_{70} layer, the C_{60} molecules seek a three-fold hollow site and result in a strain at such an interface. This is because of C_{60} under tensile stress and C_{70} under compressive stress. The strain is relieved

when the C_{70} molecules take upright positions. C_{60} molecules can drop into the first layer due to the extra space created when C_{70} molecules change their orientations from free rotating to fixed upright configuration. Molecular transport between layers becomes more significant at elevated temperatures. De-wetting of the HOPG substrate takes a place at sufficiently high temperatures leading to the formation of the 3rd and 4th layers. The C_{60}-C_{70}/HOPG and C_{70}-C_{60}/HOPG systems provide an ideal model to assemble in/organic materials in a chosen sequence for developing nanoelectronics and optoelectronic devices.

Acknowledgments

Chinese Scholarship Council for providing a scholarship to Lu'an Guo. Special thanks to Dogan Kaya who generously volunteered his time and expertise during the revision. The authors also acknowledge the support from the National Key Research and Development Program (No. 2019YFB2203400), UESTC Shared Research Facilities of Electromagnetic Wave and Matter Interaction (Y0301901290100201) and Young Scientists Fund of the Basic and Applied Basic Research of Guangdong (2019A1515110021).

References

[1] H.P. Schultz, Topological organic chemistry. Polyhedranes and prismanes, J. Org. Chem. 30 (1965) 1361–1364. https://doi.org/10.1021/jo01016a005.

[2] H.W. Kroto, J.R. Heath, S.C. O'Brien, R.F. Curl, R.E. Smalley, C60: buckminsterfullerene, Nature. 318 (1985) 162–163. https://doi.org/10.1038/318162a0.

[3] H.P. Boehm, A. Clauss, G.O. Fischer, U. Hofmann, Das Adsorptionsverhalten sehr dünner Kohlenstoff-Folien, Zeitschrift Für Anorg. Und Allg. Chemie. 316 (1962) 119–127. https://doi.org/10.1002/zaac.19623160303.

[4] E.A. Rohlfing, D.M. Cox, A. Kaldor, Production and characterization of supersonic carbon cluster beams, J. Chem. Phys. 81 (1984) 3322–3330. https://doi.org/10.1063/1.447994.

[5] K. Prassides, H.W. Kroto, R. Taylor, D.R.M. Walton, W.I.F. David, J. Tomkinson, R.C. Haddon, M.J. Rosseinsky, D.W. Murphy, Fullerenes and fullerides in the solid state: Neutron scattering studies, Carbon N. Y. 30 (1992) 1277–1286. https://doi.org/10.1016/0008-6223(92)90068-8.

[6] K. HEDBERG, L. HEDBERG, D.S. BETHUNE, C.A. BROWN, H.C. DORN, R.D. JOHNSON, M. DE VRIES, Bond Lengths in Free Molecules of Buckminsterfullerene, C60, from Gas-Phase Electron Diffraction, Science (80-.). 254 (1991) 410–412. https://doi.org/10.1126/science.254.5030.410.

[7] D.R.R. McKenzie, C.A.A. Davis, D.J.H.J.H. Cockayne, D.A.A. Muller, A.M.M. Vassallo, The structure of the C70 molecule, Nature. 355 (1992) 622–624. https://doi.org/10.1038/355622a0.

[8] E. V. Shevchenko, D. V. Talapin, A. L. Rogach, A. Kornowski, M. Haase, H. Weller, Colloidal Synthesis and Self-Assembly of CoPt3 Nanocrystals, J. Am. Chem. Soc. 124 (2002) 11480–11485. https://doi.org/10.1021/ja025976l.

[9] F.X. Redl, K.-S. Cho, C.B. Murray, S. O'Brien, Three-dimensional binary superlattices of magnetic nanocrystals and semiconductor quantum dots, Nature. 423 (2003) 968–971. https://doi.org/10.1038/nature01702.

[10] A.R. McGhie, J.E. Fischer, P.A. Heiney, P.W. Stephens, R.L. Cappelletti, D.A. Neumann, W.H. Mueller, H. Mohn, H.-U. ter Meer, Phase transitions in solid C70: Supercooling, metastable phases, and impurity effect, Phys. Rev. B. 49 (1994) 12614–12618. https://link.aps.org/doi/10.1103/PhysRevB.49.12614.

[11] J.L. Sauvajol, Z. Hricha, N. Coustel, Z. Zahab, R. Aznar, Photoluminescence of solid C60, J. Phys. Condens. Matter. 5 (1993) 2045–2054.

[12] H.N. Aiyert, A. Govindaraj, C.N.R. Rao, Orientational disorder and other aspects of C70 and C60[sbnd]C70 films deposited on single-crystal substrates, Philos. Mag. Lett. 72 (1995) 185–191. https://doi.org/10.1080/09500839508242450.

[13] J. Wragg, J. Chamberlain, H. White, Scanning tunnelling microscopy of solid C60/C70, Nature. 348 (1990) 623. https://doi.org/10.1038/348623a0.

[14] K. Sato, T. Tanaka, K. Akaike, K. Kanai, Morphological phase diagrams of C60 and C70 films on graphite, Surf. Sci. 664 (2017) 222–225. https://doi.org/10.1016/j.susc.2017.06.018.

[15] R. Mirzayev, K. Mustonen, M.R.A. Monazam, A. Mittelberger, T.J. Pennycook, C. Mangler, T. Susi, J. Kotakoski, J.C. Meyer, Buckyball sandwiches, Sci. Adv. 3 (2017). https://doi.org/10.1126/sciadv.1700176.

[16] M.-Y. Li, C.-H. Chen, Y. Shi, L.-J. Li, Heterostructures based on two-dimensional layered materials and their potential applications, Mater. Today. 19 (2016) 322–335. https://doi.org/https://doi.org/10.1016/j.mattod.2015.11.003.

[17] H. Gonzalez Herrero, Probing and manipulating graphene physics at the atomic level,

Universidad Autónoma de Madrid, 2016.

[18] M. Gruenewald, L.K. Schirra, P. Winget, M. Kozlik, P.F. Ndione, A.K. Sigdel, J.J. Berry, R. Forker, J.-L. Brédas, T. Fritz, O.L.A. Monti, Integer Charge Transfer and Hybridization at an Organic Semiconductor/Conductive Oxide Interface, J. Phys. Chem. C. 119 (2015) 4865–4873. https://doi.org/10.1021/jp512153b.

[19] Y.C. Xie, M. Rokni Fard, D. Kaya, D. Bao, R.E. Palmer, S. Du, Q. Guo, Site-specific assembly of fullerene nanorings guided by two-dimensional gold clusters, J. Phys. Chem. C. 120 (2016) 10975–10981. https://doi.org/10.1021/acs.jpcc.6b02798.

[20] X. Zhang, L. Tang, Q. Guo, Low-temperature growth of C60 monolayers on Au(111): island orientation control with site-selective nucleation, J. Phys. Chem. C. 114 (2010) 6433–6439.

[21] H.M. Rhoda, M.P. Kayser, Y. Wang, A.Y. Nazarenko, R. V Belosludov, P. Kiprof, D.A. Blank, V.N. Nemykin, Tuning Up an Electronic Structure of the Subphthalocyanine Derivatives toward Electron-Transfer Process in Noncovalent Complexes with C60 and C70 Fullerenes: Experimental and Theoretical Studies, Inorg. Chem. 55 (2016) 9549–9563. https://doi.org/10.1021/acs.inorgchem.6b00992.

[22] H. Ma, H. Babaei, Z. Tian, The importance of van der Waals interactions to thermal transport in Graphene-C60 heterostructures, Carbon N. Y. 148 (2019) 196–203. https://doi.org/https://doi.org/10.1016/j.carbon.2019.03.076.

[23] S. Fu, L. Qin, X. Zhang, R. Wang, D. Tang, X. Qiu, Interfacial optoelectronic process in organic-inorganic van der Waals hetero-structure, Chinese Sci. Bull. 64 (2019) 393–410. https://doi.org/https://doi.org/10.1360/N972018-00985.

[24] A.S. Komolov, E.F. Lazneva, N.B. Gerasimova, Y.A. Panina, G.D. Zashikhin, A.V. Baramygin, P. Si, S.N. Akhremtchik, A.A. Gavrikov, Density of the unoccupied electronic states of the ultrathin films of the aziridinylphenylpyrrol substituted fullerene, J. Electron Spectros. Relat. Phenomena. 205 (2015) 52–56. https://doi.org/10.1016/j.elspec.2015.08.002.

[25] A.S. Komolov, E.F. Lazneva, S.N. Akhremtchik, N.S. Chepilko, A.A. Gavrikov, Unoccupied Electronic States at the Interface of Oligo(phenylene-vinylene) Films with Oxidized Silicon, J. Phys. Chem. C. 117 (2013) 12633–12638. https://doi.org/10.1021/jp4027223.

[26] A.L. Shu, W.E. McClain, J. Schwartz, A. Kahn, Interface dipole engineering at buried organic–organic semiconductor heterojunctions, Org. Electron. 15 (2014) 2360–2366. https://doi.org/https://doi.org/10.1016/j.orgel.2014.06.039.

[27] R.D. Johnson, G. Meijer, D.S. Bethune, C60：has icosahedral symmetry, J. Am. Chem. Soc. 112 (1990) 8983–8984. https://doi.org/10.1021/ja00180a055.

[28] L. Guo, Y. Wang, D. Kaya, R.E. Palmer, G. Chen, Q. Guo, Orientational Epitaxy of van der Waals Molecular Heterostructures, Nano Lett. 18 (2018) 5257–5261. https://doi.org/10.1021/acs.nanolett.8b02238.

[29] L.A. Ponomarenko, A.K. Geim, A.A. Zhukov, R. Jalil, S. V Morozov, K.S. Novoselov, I. V Grigorieva, E.H. Hill, V. V Cheianov, V.I. Fal'ko, K. Watanabe, T. Taniguchi, R. V Gorbachev, Tunable metal–insulator transition in double-layer graphene heterostructures, Nat. Phys. 7 (2011) 958. https://doi.org/10.1038/nphys2114.

[30] S.J. Haigh, A. Gholinia, R. Jalil, S. Romani, L. Britnell, D.C. Elias, K.S. Novoselov, L.A. Ponomarenko, A.K. Geim, R. Gorbachev, Cross-sectional imaging of individual layers and buried interfaces of graphene-based heterostructures and superlattices, Nat. Mater. 11 (2012) 764. https://doi.org/10.1038/nmat3386.

[31] A.K. Geim, I. V. Grigorieva, Van der Waals heterostructures, Nature. 499 (2013) 419–425. https://doi.org/10.1038/nature12385.

[32] K.J. Franke, G. Schulze, J.I. Pascual, Excitation of Jahn−Teller Active Modes during Electron Transport through Single C60 Molecules on Metal Surfaces, J. Phys. Chem. Lett. 1 (2010) 500–504. https://doi.org/10.1021/jz900260v.

[33] X.-Q. Shi, M.A. Van Hove, R.-Q. Zhang, Adsorbate-induced reconstruction by C${}_{60}$ on close-packed metal surfaces: Mechanism for different types of reconstruction, Phys. Rev. B. 85 (2012) 75421. https://doi.org/10.1103/PhysRevB.85.075421.

[34] J. Guan, J. Wu, D. Jiang, X. Zhu, R. Guan, X. Lei, P. Du, H. Zeng, S. Yang, Hybridizing MoS2 and C60 via a van der Waals heterostructure toward synergistically enhanced visible light photocatalytic hydrogen production activity, Int. J. Hydrogen Energy. 43 (2018) 8698–8706. https://doi.org/https://doi.org/10.1016/j.ijhydene.2018.03.148.

[35] J. Cho, J. Smerdon, L. Gao, Ö. Süzer, J.R. Guest, N.P. Guisinger, Structural and Electronic Decoupling of C60 from Epitaxial Graphene on SiC, Nano Lett. 12 (2012) 3018–3024. https://doi.org/10.1021/nl3008049.

[36] M. Drechsler, J.J. Métois, J.C. Heyraud, Surface self-diffusion studied by microscopic measurements of crystallite profile evolutions, Surf. Sci. 108 (1981) 549–560. https://doi.org/10.1016/0039-6028(81)90564-1.

[37] K. Kim, T.H. Lee, E.J.G. Santos, P.S. Jo, A. Salleo, Y. Nishi, Z. Bao, Structural and Electrical Investigation of C60–Graphene Vertical Heterostructures, ACS Nano. 9 (2015) 5922–5928. https://doi.org/10.1021/acsnano.5b00581.

[38] P. Gravil, M. Devel, P. Lambin, X. Bouju, C. Girard, A. Lucas, Adsorption of C60 molecules, Phys. Rev. B. 53 (1996) 1622–1629. https://doi.org/10.1103/PhysRevB.53.1622.

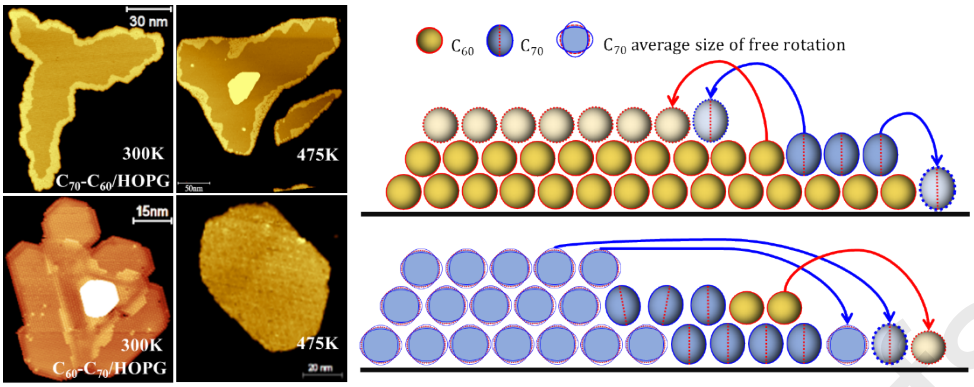
[39] S. Szuba, R. Czajka, A. Kasuya, A. Wawro, H. Rafii-Tabar, Observation of C60 film formation on a highly oriented pyrolitic graphite substrate via scanning tunnelling microscopy, Appl. Surf. Sci. 144–145 (1999) 648–652. https://doi.org/10.1016/S0169-4332(98)00887-3.

[40] T.T. Tsong, Effects of an electric field in atomic manipulations, Phys. Rev. B. 44 (1991) 13703–13710. http://link.aps.org/doi/10.1103/PhysRevB.44.13703.

[41] D. Kaya, The effect of electric field on a fullerene molecule on a metal surface by a nano STM tip, Phys. B Condens. Matter. 557 (2019) 126–131. https://doi.org/https://doi.org/10.1016/j.physb.2019.01.026.

Journal Pre-proofs

Graphical Abstract



Journal Pre-proofs

Journal Pre-proofs

Highlights

1. Build C_{60}-C_{70} molecular heterojunctions with high designable and efficiency processing.
2. The introduced C_{70} molecules are standing up configuration with its long molecular axis perpendicular to the substrate.
3. The lateral/vertical van der Waals heterostructure can be built with simple thermo activity.

Journal Pre-proofs

Lu'an Guo: Conceptualization, Validation, Formal analysis, Investigation, Writing - Original Draft, Visualization.

Yitao Wang: Formal analysis, Investigation.

Dogan Kaya: Formal analysis, Investigation, Writing - Review & Editing.

Zhiming Wang: Co-Supervision, Writing – Review, Funding acquisition.

Min Zhang: Co-Supervision, Writing – Review, Funding acquisition.

Quanmin Guo: Main Supervision, Conceptualization, Methodology, Writing - Review & Editing, Funding acquisition.

Journal Pre-proofs

Declaration of interests

☒ The authors declare that they have no known competing financial interests or personal relationships that could have appeared to influence the work reported in this paper.

☐The authors declare the following financial interests/personal relationships which may be considered as potential competing interests:

Journal Pre-proofs